Materials Science & Engineering C 81 (2017) 156–166

Contents lists available at ScienceDirect

Materials Science & Engineering C

journal homepage: www.elsevier.com/locate/msec

Electrochemical preparation and characterization of PNIPAM-HAp scaffolds for bone tissue engineering

Charlene Aparecida Ribeiro[a], Marcos Vinicius Surmani Martins[b], Ana Helena Bressiani[b], José Carlos Bressiani[b], Maria Elena Leyva[c,d], Alvaro Antonio Alencar de Queiroz[c,d,*]

[a] Post Graduate Program in Materials for Engineering, Federal University of Itajubá (UNIFEI) (UNIFEI), Av. BPS 1303, 37500-903 Itajubá, MG, Brazil
[b] Science and Materials Technology Center (CCTM) (IPEN/CNEN), Av. Professor Lineu Prestes 2242, 05508-000 São Paulo, SP, Brazil
[c] Physics and Chemistry Institute (IFQ), Federal University of Itajubá (UNIFEI), Av. BPS 1303, 37500-903 Itajubá, MG, Brazil
[d] High Voltage Laboratory (LAT-EFEI), Federal University of Itajubá (UNIFEI), Av. BPS 1303, 37500-903 Itajubá, MG, Brazil

ARTICLE INFO

Keywords:
Electrochemical polymerization
Poly(*N*-isopropylacrylamide)
Hydroxyapatite
Thermoresponsive scaffolds
Bone tissue engineering
Oxacillin

ABSTRACT

In the last decade, a variety of methods for fabrication of three-dimensional biomimetic scaffolds based on hydrogels have been developed for tissue engineering. However, many methods require the use of catalysts which compromises the biocompatibility of the scaffolds. The electrochemical polymerization (ECP) of acrylic monomers has received an increased attention in recent years due to its versatility in the production of highly biocompatible coatings for the electrodes used in medical devices. The main aim of this work was the use of ECP as scaffold fabrication technique to produce highly porous poly(*N*-isopropylacrylamide) (PNIPAM)/hydroxyapatite (HAp) composite for bone tissue regeneration. The prepared PNIPAM-HAp porous scaffolds were characterized by SEM, FTIR, water swelling, porosity measurements and X-ray diffraction (XRD) techniques. FTIR indicates that ECP promotes a successful conversion of NIPAM to PNIPAM. The water swelling and porosity were shown to be controlled by the HAp content in PNIPAM-HAp scaffolds. The PNIPAM-HAp scaffolds exhibited no cytotoxicity to MG63 cells, showing that ECP are potentially useful for the production of PNIPAM-HAp scaffolds. To address the osteomyelitis, a significant complication in orthopedic surgeries, PNIPAM-HAp scaffolds were loaded with the antibiotic oxacillin. The oxacillin release and the bacterial killing activity of the released oxacillin from PNIPAM-HAp against *S. aureus* and *P. aeruginosa* were demonstrated. These observations demonstrate that ECP are promising technique for the production of non-toxic, biocompatible PNIPAM-HAp scaffolds for tissue engineering.

1. Introduction

Nowadays, the high performance of synthetic biomaterials and the availability of high technology to design and processing polymer composites into scaffolds have revolutionized the field of bone tissue engineering. The design and processing of polymeric composites into scaffolds is indispensable for the modern regenerative medicine and contributes significantly to the health economy and medical care of developed countries [1–4].

For several decades hydrogel's scaffolds have received a considerable attention due to their unique compositional and structural similarities to the natural extracellular matrix (ECM) due to their tunable porous structure for cellular proliferation and survival making them the ideal materials for tissue engineering [5–7]. In addition, the mass transport properties of scaffolds based hydrogels may potentially offer selectivity over nutrient uptake and metabolites or even influence the cellular growth based on the physical properties of the surrounding hydrogel environment that has been pre-seeded with biological cells [8,9].

Poly(*N*-isopropylacrylamide) (PNIPAM) is one of the most widely studied thermo-responsive hydrogel in the field of bone tissue engineering [10–14]. PNIPAM responds according to the temperature changes and exhibits lower critical solution temperature (LCST) around 32 °C [15,16]. PNIPAM has a hydrophobic core with a hydrophilic outer shell so that when the LCST is exceeded the thermoresponsive polymer forms a compact precipitate in the aqueous environment [17,18].

The advances in the development of bioactive scaffolds taking advantages of the LCST of PNIPAM are particularly relevant for the field of tissue engineering. However, despite their potential use in bone

* Corresponding author at: Institute of Physics and Chemistry - IFQ, High Voltage Laboratory (LAT-EFEI), Federal University of Itajubá – UNIFEI, Av. BPS 1303, 37500-903 Itajubá, MG, Brazil.
E-mail address: alencar@unifei.edu.br (A.A.A. de Queiroz).

http://dx.doi.org/10.1016/j.msec.2017.07.048
Received 4 August 2016; Received in revised form 18 May 2017; Accepted 29 July 2017
Available online 31 July 2017
0928-4931/

tissue engineering applications, PNIPAM hydrogels have not achieved clinical acceptance due to their cytotoxic behavior that represent a regulatory barrier to its medical use [19–23].

PNIPAM has been synthesized by a variety of techniques wherein in the last decade three methods of controlled free radical polymerization have gained attention in the synthesis of well-defined polymers with controlled molecular weights and narrow molecular weight distributions. These methods include nitroxide-mediated polymerization (NMP), atom transfer radical polymerization (ATRP) and reversible addition fragmentation chain transfer (RAFT) polymerization [24–26].

The techniques NMP, ATRP and RAFT are significantly amenable relatively to the radical thermal redox, ionizing radiations and photochemical initiated NIPAM polymerizations [27–31]. Unfortunately, impurities as the residual monomer, catalysts and initiators from the NIPAM polymerization reaction medium may seriously adversely affect the biocompatible properties of PNIPAM hydrogels [32–34].

Although PNIPAM are commonly synthesized through the use of chemical initiators or catalysts, it became clear that the thermoresponsive polymer can also be obtained by electrochemical polymerization (ECP) [35–36]. Both chemical synthesis and ECP refers to oxidative polymerization processes. However, the ECP method involves the direct oxidation of the NIPAM at the anode, without the need for initiators or catalysts, resulting in suitable biocompatible properties of the resultant hydrogel for the production of scaffolds for tissue engineering [37–38].

More recently, bone tissue engineering strategies have focused on fabricating scaffolds based on hydrogel-hydroxyapatite scaffolds [39–42]. Hydroxyapatite (HAp, $Ca_{10}(PO_4)_6(OH)_2$) is the most favorable ceramic for the production of bone tissue engineering scaffolds due to its excellent biocompatibility and composition that mimics the bone tissue microstructure [43].

In spite of the large number of investigations about PNIPAM hydrogels, as far as the authors are aware, no investigations about the use of ECP technique to obtain PNIPAM-HAp scaffolds with antimicrobial property were reported till the moment. Compared to traditional hydrogel-HAp composites, PNIPAM-HAp scaffolds offer great advantages for bone tissue engineering. Instead of acting passively as a hydrogel composite material, they will interact and respond to the environmental setting actuating as gates according to biological environment. Originally, the advantages of fabrication of PNIPAM-bioceramic composites are usually for the purpose to give to the porous structure of the PNIPAM-HAp the role of chemical valves that regulates the flow of water and the molecular diffusion of solutes through scaffolds. This strategy would be interesting to develop dynamical hydrogel-HAp scaffolds for the regeneration bone tissue.

The purpose of this work was to study the use of ECP technique to produce PNIPAM-HAp scaffolds with controlled release properties of oxacillin, a commonly β-lactamic antibiotic used in orthopedic surgeries for treatment of bone infections [44]. The PNIPAM-HAp scaffolds prepared through ECP were characterized by scanning electron microscopy (SEM), Fourier transform infrared spectroscopy (FTIR), X-ray diffraction (DRX), thermogravimetric analysis (TGA), porosity measurements and water swelling behavior. The influence of the addition of the HAp on the microstructure of PNIPAM hydrogel and their potential effect on the release of oxacillin from PNIPAM-HAp scaffolds were examined.

2. Materials and methods

2.1. Materials

The monomer *N*-isopropylacrylamide (NIPAM) and the crosslinking agent 2-methylene-bis-acrylamide (MBA) were purchased from Sigma-Aldrich Chemical Co (Brazil). NIPAM was purified by recrystallization from toluene:n-hexane (1:3) mixture and then dried in a vacuum oven at room temperature (25 °C). A synthetic hydroxyapatite HAP-91® powder (HAp) with particles sizes around 10 μm was purchased from JHS Biomaterials (Brazil). The composition of HAP-91® used in this work was 70% (w/w) of HAp and 30% (w/w) of β-tricalcium phosphate (β-TCP). The Ca:P atomic ratios for HAP-91® determined from inductively coupled plasma (ICP) spectroscopy analysis was 1.75 ± 0,04 and their XRD patterns (Fig. 6) confirmed the presence of HAp crystalline phase by comparing the data obtained with the ICDD - PDF2 card: 00-009-0432. All of the solutions were prepared using distilled and deionized water (64.1 MΩ) and were purged with nitrogen gas (25 mL·min^{-1}) for 20 min to remove dissolved oxygen prior to ECP.

2.2. Synthesis of PNIPAM-HAp by ECP and scaffold preparation

Porous PNIPAM-HAp scaffolds with HAp content of 30% w/w (PNIPAM-HAp_{30}), 50% w/w (PNIPAM-HAp_{50}) and 60% w/w (PNIPAM-HAp_{60}) in 1.00 g of total mass of PNIPAM were synthesized using ECP method. A mixture of 1.0 g of the NIPAM monomer was added to 10 mL of bi-distilled water (1.0 M monomer/solvent) along with 50 mM of MBA as crosslinker to produce a three dimensional scaffold PNIPAM-HAp network. An appropriate amount of HAp (300, 500 and 600 mg) was added to NIPAM monomer aqueous solution followed by ultrasonic dispersion for 10 min at room temperature (25 °C) to form a NIPAM-HAp uniform mixture. The viscosity of aqueous NIPAM-HAp suspensions were made with a Brookfield viscometer (LVDV-II with adapter for small volumes, spindle SC4-18) at room temperature (25 °C).

The ECP of the NIPAM-HAp was carried out in a single-compartment electrochemical cell (EC) with the electrodes connected to an Omnimetra PG39M electrochemical workstation as shown in the Fig. 1.The ECP experiments were performed using the galvanostatic method under a constant current of 100 mA at room temperature (25 °C). The working electrode (WE) was a silver sheet with dimensions of 1.0 cm length and 0.5 cm width. The auxiliary (counter) electrode (CE) was a platinum foil with the same dimensions of the WE. Before each run both, the WE and the CE were cleaned and washed thoroughly with water, double distilled water, rinsed with ethanol and dried under vacuum at room temperature (25 °C). The EC cell was bubbled with nitrogen gas for 10 min prior the ECP reaction. After ECP, PNIPAM-HAp scaffolds were removed from the EC cell and purified by swelling-deswelling method to remove the unreacted chemicals. The equilibrium of swelling of PNIPAM-HAp scaffolds was carried out in distilled water at 25 °C at least for 2 days that was refreshed daily. Then, the equilibrium water swollen at 25 °C PNIPAM-HAp scaffolds were transferred into hot distilled water (50 °C). The swelling-deswelling procedure of PNIPAM-HAp was repeated for 5 days; finally the scaffolds were dried in a hot air oven at 60 °C until constant weight. The percentage of NIPAM-HAp conversion to PNIPAM-HAp was determined gravimetrically from the ratio between the amount of NIPAM-HAp initially introduced in the EC and the amount of the PNIPAM-HAp produced after ECP.

The scaffold samples were prepared by swollen PNIPAM-HAp in distilled and deionized water at 25 °C until equilibrium followed by

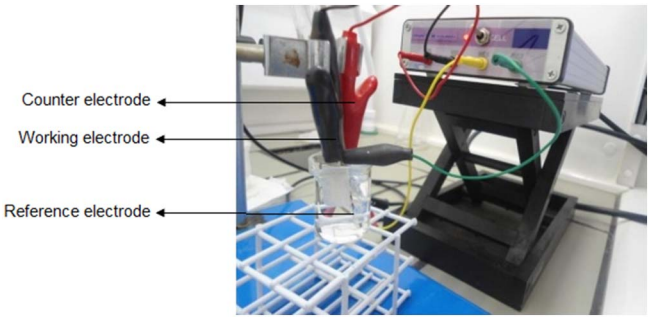

Fig. 1. The electrochemical cell used in the ECP of NIPAM-HAp solutions for the synthesis of PNIPAM-HAp scaffolds. The ECP reaction was conducted at 25 °C, normal pressure (101,3 kPa) and 100 mA.

freezing at − 20 °C and kept at this temperature for 24 h. The frozen PNIPAM-HAp scaffolds were subjected to the process of lyophylization, where freeze drying was carried out under vacuum at the temperature of − 80 °C.

2.3. Physical-chemical characterization of PNIPAM-HAp scaffolds

The microstructure, porous size and morphology of the produced PNIPAM-HAp scaffolds were studied by using a scanning electron microscopy (SEM) type Phillips-XL 30, operating at 20 kV. The PNIPAM-HAp scaffolds prior to SEM observation were gold sputtered. The ImageJ software was used for the determination of pore dimensions. The average value was considered of the measurements of 600 pores.

The presence of the expected functional groups associated to the presence of PNIPAM and HAp in the PNIPAM-HAp scaffolds was confirmed by FTIR spectroscopy. The FTIR spectra of PNIPAm-HAp composites were recorded on a Perkin Elmer Spectrum 100 FTIR spectrometer at resolution of 2 cm^{-1}, in the range of 4000–650 cm^{-1} by using attenuated total reflectance accessory (ATR) with 64 scans.

The crystalline phases of the PNIPAM-HAp scaffolds were determined by X-ray diffraction (XRD) using a Rigaku X-ray diffractometer with CuKα radiation source over the 2θ range of 10° to 50° with a step size of 0.05°.

Porosity is one of the important parameter in the design and performance of scaffolds. The appropriate porosity will be making the PNIPAM-HAp composite suitable for its applications as biomaterial. The porosity of the PNIPAM-HAp scaffolds was measured by liquid displacement method. The alkane n-heptane (n-C_7H_{16}) with density ρ was used as a displacement liquid because it can easily penetrate the scaffolds and would not induce shrinking or swelling as a non-solvent of the PNIPAM-HAp. The scaffolds, pycnometer and n-C_7H_{16} were kept at 25 °C for 1 h before testing. The weight of dry PNIPAM-HAp was immersed into the pycnometer filled with n-C_7H_{16} for 24 h until all the air in the scaffold was removed. The PNIPAM-HAp scaffolds saturated with n-C_7H_{16} were removed from the pycnometer and the weight of the residual alkane and pycnometer was measured. The porosities of PNIPAM-HAp scaffolds were determined from Eq. (1) [45]:

$$P(\%) = \frac{(W_2 - W_1)}{(\rho V_1)} \cdot 100 \quad (1)$$

where W_2 is the saturation mass of the sample after immersion, W_1 is the initial mass of the sample, V_1 is the volume of the sample prior to immersion into pycnometer filled with n-C_7H_{16} and ρ is the density of n-C_7H_{16} at 25 °C (684 kg/m^3).

Thermogravimetric analyses (TGA) of PNIPAM-HAp samples were performed using a thermogravimetric Analyzer (model TGA-50, Shimadzu Co) in order to record the thermal effects during heating of scaffolds. PNIPAM-HAp scaffolds weighing approximately 5 mg were placed in an Al_2O_3 crucible, and heated at a rate of 10 °C·min^{-1} from 25 °C to 1000 °C in a nitrogen atmosphere at flow rate of 40 mL·min^{-1}.

It is well known that swelling of the pure PNIPAM hydrogels demonstrate a sharp transition at the temperature of about 30–32 °C caused by hydrophobic attraction related to the dehydration of the gel [15]. However, due to charge repulsion and enhanced osmotic pressure in the media, the phase transition of PNIPAM is not completed at 32 °C but around 40 °C [15,16]. Thus, the swelling behavior of the PNIPAM-HAp were measured by immersing a dry scaffold sample of known weight in distilled and deionized water at 25 °C and 40 °C by specific time period. After a defined time interval, the swollen hydrogels were taken out from the swelling media, and weighed periodically after carefully drying its surface with a filter paper. The equilibrium water swelling ratio (Q) was calculated according to Eq. (2):

$$Q = \frac{W_e}{W_d} \quad (2)$$

where W_e is the weight of the swollen PNIPAm-HAp sample at equilibrium time t, W_d is weight of the dry PNIPAM-HAp sample.

Dynamic swelling experiments were performed by placing the PNIPAM-HAp scaffolds in distilled and deionized water at 37.0 ± 0.1 °C (in a thermostatic bath) and measuring their weight gain as a function of time. The swollen PNIPAM-HAp scaffolds samples were weighed after blotting with a filter paper to remove the surface water. The water swelling degree (W_S (%)) was calculated using the Eq. (3):

$$W_S = \frac{(m - m_o)}{m_o} \cdot 100 \quad (3)$$

where m_o and m are the weights of the initial dry PNIPAM-HAp and swollen scaffolds, respectively.

2.4. Cytotoxicity characterization

Studies about the cell viability in the presence of PNIPAM-HAp scaffolds were performed using the MTT test [46]. The PNIPAM-HAp scaffolds were first immersed in the culture medium (Dulbecco Modified Eagle's Medium, DMEM) at concentration of 1.0 cm^2·mL^{-1} and incubated at 37 °C, 5% CO_2 in air for 72 h to obtain the extract media to assess the cytotoxicity as a result of some extractable residual chemical compound or foreign particulates presents on scaffolds. After filtration to remove the PNIPAM-HAp scaffolds the test solution was termed in this work as extract concentration.

The MG63 cells (ATCC CRL-1427, USA) were cultured in DMEM containing penicillin/streptomycin and L-glutamine (0.2 mol·L^{-1}) and supplemented with 10% fetal bovine serum. The cells were incubated at 37 °C in a 95% humidified atmosphere containing 5% CO_2.

The MG63 cells were re-suspended in culture medium and plated in 24-well plates at a density of $3.0.10^4$ cells·mL^{-1} and then incubated for 24 h in a humidified atmosphere of 5% CO_2. Thereafter, the medium was replaced with 1 mL of the test solution. The culture medium was used as negative control and phenol 0.3% (m/v) in phosphate buffer saline (PBS) pH 7.4, as positive control. Following 24 h of incubation, the test solutions were removed, and each well was treated with 10 μL of 3-(4,5-dimethylthiazol-2-yl)-2,5-diphenyl tetrazolium bromide (MTT) (5 mg·mL^{-1} in PBS) and incubated for 4 h at 37 °C in a humidified atmosphere of 5% CO_2. The yellow MTT was reduced to blue-purple formazan in the presence of the mitochondrial dehydrogenase present in intact living MG63 cells and the blue-purple color produced should be proportional to the number of viable cells present. The MTT solution was then replaced with 100 μL/well of dimethyl sulfoxide (DMSO) to dissolve the formazan salts, followed by 10 min of slow agitation, yielding a blue-purple solution. The absorbance of this solution was measured at 570 nm and 690 nm (reference) using a microplate (ELISA) reader. The MTT assay was performed in triplicate.

2.5. Oxacillin loading into PNIPAM-HAp scaffolds

The antibiotic oxacillin (5 methyl-3 phenyl-4-isoxazolyl penicillin sodium salt) was incorporated into PNIPAM-HAp scaffolds, and its release behavior was investigated in vitro. The scaffolds loaded with oxacillin were prepared by direct addition of 250 mg·mL^{-1} of PNIPAM-HAp scaffolds to 8.03 mg·mL^{-1} (20.10^{-3} mol·L^{-1}) of oxacillin previously dissolved in phosphate buffer saline solution (PBS 10 mM, pH 7.4, 150 mM NaCl, 40 mM NaH_2PO_4 and 40 mM NaOH) for 24 h at 25 °C followed by lyophilization. The amount of oxacillin loaded inside PNIPAM-HAp scaffolds were analyzed by UV–Vis spectrophotometry (UV–Vis, Cary 50), using the absorption calibration curves generated at 205 nm from the oxacillin standard solutions at known concentrations. The drug loading (DL) and incorporation efficiency (IE) of the PNIPAM-HAp scaffolds were calculated based on the Eqs. (4) and (5), respectively.

$$DL(\%) = \frac{\text{Oxacillin weight in scaffold}}{\text{Scaffold weight}} \cdot 100 \quad (4)$$

$$IE(\%) = \frac{\text{Oxacillin weight in scaffold}}{\text{Initial weight of oxacillin}} \cdot 100 \quad (5)$$

2.6. In vitro oxacillin release studies

The oxacillin-loaded PNIPAM-HAp scaffolds were immersed in 10 mL of PBS pH 7.4 in a temperature-controlled shaker and the temperature effect on oxacillin delivery from PNIPAM-HAp scaffolds were studied at 25 °C and 37 °C by using the Arrhenius equation for the determination of activation energy (E_A). If the E_A is known useful information about molecular motion of oxacillin in PNIPAM-HAp scaffolds can be obtained. Samples were withdrawn at regular time intervals, and the same volume was replaced with fresh PBS pH 7.4 solution. The samples were spectrophotometrically measured at 205 nm. Cumulative oxacillin release ($CO_xR(\%)$) was determined from the Eq. (6):

$$CO_xR(\%) = \frac{V_o \cdot C_n + V_E \sum_1^{n-1} C_i}{m} \cdot 100 \quad (6)$$

where V_o is the volume of release medium (10 mL), V_e is the volume of release media taken out every time (3 mL), C_i is the concentration of oxacillin released from PNIPAM-HAp scaffolds at intervals of i, m is the mass of oxacillin loading, and n is the replacement times.

All the measurements were done in triplicate, and the data points represent the mean ± SD from independent experiments.

2.7. Inhibitory effectiveness of released oxacillin

The inhibitory effectiveness of the released oxacillin from PNIPAM-HAp scaffolds was assayed by turbidimetry method using *S. aureus* (ATCC 12598) and *P. aeruginosa* (ATCC 27317). The protocol assay was adapted from the Clinical and Laboratory Standard Method M07-A9 [47]. Briefly, 200 μL of the PNIPAM-HAp scaffold eluates were added to sterile tubes containing 1.75 mL Trypticase soy broth (TSB) and inoculated with 2.0×10^4 colony forming units (CFU) of *S. aureus* and *P. aeruginosa* respectively. Turbidity was determined spectrophotometrically at 530 nm after 24 h incubation at 37 °C.

2.8. Statistics

The difference between the testing groups using one-way ANOVA (analysis of variance) was performed. A significant difference was considered when p-value was 0.05 or less, indicating 95% confidence limit.

3. Results and discussion

3.1. Synthesis of PNIPAM-HAp by ECP and scaffolds preparation

The electrochemical synthesis of PNIPAM refers to the oxidation of the NIPAM monomer and growth of the thermoresponsive polymer chain onto anode surface. Since the oxidation is carried out by applying a positive potential or current, the ECP avoids the use of chemical oxidants, thus achieving greater purity of the desired PNIPAM.

The first step of the mechanism of ECP appears to be the oxidation reaction of NIPAM with the formation of both, carbocations and macrocarbocations attacking the monomer (NIPAM) and crosslinker (MBA) simultaneously to form the N-localized radicals [48]. The N-localized radicals can trigger a cascade of reactions that typically involve the loss of a proton and the formation of C-localized radicals, which would then initiate the polymerization by attacking simultaneously the vinyl groups of the NIPAM and MBA, favoring the polymerization process at low temperatures. The ECP mechanism for the synthesis of PNIPAM is illustrated in Scheme 1.

Fig. 2(A) shows the progression of ECP expressed as the conversion of NIPAM to PNIPAM versus time for the NIPAM-HAp mixture. The NIPAM-HAp dispersions were stable throughout ECP period and would tend to trap more radicals occluding more unreacted monomer (NIPAM) during ECP processes thus lowering the degree of polymerization conversion. However, the presence of the HAp particles in concentrations as higher as 50% (w/w) does not appears to reduce significantly the conversion degree of NIPAM to PNIPAM (Fig. 2(A)). This result is most likely due to the result of the easy mechanism of electric charge transport across the interface of each grain and the electrical properties of HAp [49].

Fig. 2(B) compares the average molecular weight (M_N) and polydispersion index (PDI = $\frac{M_W}{M_N}$) of soluble fraction of PNIPAM hydrogel measured by means of gel permeation chromatography (GPC). It can be seen that PDI increased at the increasing MBA/NIPAM ratio probably due to the decrease in the kinetic chain length of the PNIPAM chains. However, M_w of most PNIPAM obtained in the ECP reaction at 25 °C for 24 h exceeds 2.1×10^6 Da at $0 < 0.068 < 0.187$ interval of MBA/NIPAM ratio. A concomitant reduction in polydispersity index (PDI) was observed for MBA/NIPAM ≥ 0.15 mol% (Fig. 2(B)) and are consistent with the inherent heterogeneous nature of the intramolecular cross-linking process and/or the potential presence of marginal cross-coupling between PNIPAM and MBA chains. The presence of water during the ECP of NIPAM using MBA as crosslinker agent appears to decrease the kinetic chain length and the PDI, respectively, of the PNIPAM chains.

3.2. Physico-chemical characterization of PNIPAM-HAp scaffolds

3.2.1. Scanning electron microscopy (SEM) and elemental chemical analysis (EDS)

Fig. 3 shows SEM micrographs of the PNIPAM, PNIPAM-HAp_{30}, PNIPAM-HAP_{50} and PNIPAM-HAp_{60} scaffolds synthesized through ECP technique. The SEM images show that 3D pore microstructures in all PNIPAM-HAp scaffolds were heterogeneous, with pores sizes varying in the range of 3–50 μm for PNIPAM (Fig. 3(A)), 20–40 μm for PNIPAM-HAp_{30} and 16–200 μm for PNIPAM-HAp_{50} scaffolds (Fig. 3(B,C)). These results indicates that nucleation and growth of droplets of the PNIPAM-lean phase with further solidification of the PNIPAM-rich phase occurred during the ECP process. However, it was observed that an increase in the HAp concentration above 30% (w/w) decreases the scaffolds porosity. The bioceramic HAp seems to disturb the PNIPAM chains through stretching inducing the deformation of the polymeric network structure. As the HAp domains grow with increased concentration, PNIPAM chains arrange themselves to form some long-range ordering and patterns indicating the occurrence of cohesive interactions between the HAp particles themselves as well as between the HAp particles and PNIPAM chains. The pattern formation presumably occurs through multiple-point secondary chemical interactions between HAp and the PNIPAM network which lead to a significant loss of translational entropy for the bioceramic particles as well as the lowering of the conformational entropy for the polymeric chains [50].

As expected, the semiquantitative analysis of the composition of the HAp in PNIPAM matrix by EDS (Fig. 3(B,C)) showed that the PNIPAM-HAp scaffolds were composed by organic and mineral phases. The mineral phase was composed primarily of calcium and phosphorous with a Ca/P ratio estimated in 1.58 for PNIPAM-HAp scaffolds which are in the range of bone mineral composition [51].

3.2.2. Porosity measurement and water swelling studies of PNIPAM-HAp scaffolds

The measured porosity of the PNIPAM-HAp scaffolds showed in Fig. 4(I) reveals that as the amount of HAp and the MBA crosslinker are increased in feed mixture the porosity becomes low. These results indicates that the increased number of crosslinks make the PNIPAM network more compact resulting in the lowering of the mesh size

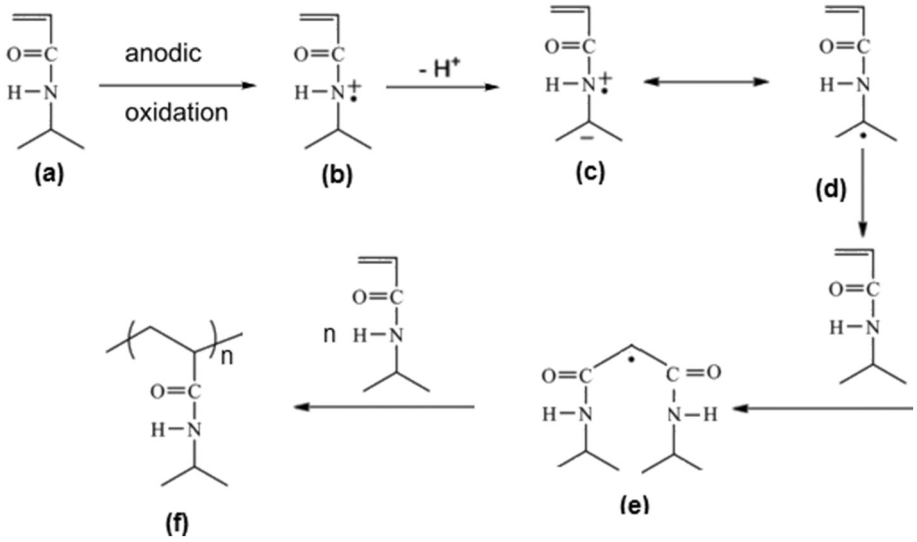

Scheme 1. Illustration of the ECP mechanism for the synthesis of PNIPAM: NIPAM monomer (a), carbocation (b), deprotonation and formation of C-localized radical (c,d), macroradical (e) and PNIPAM growth (f).

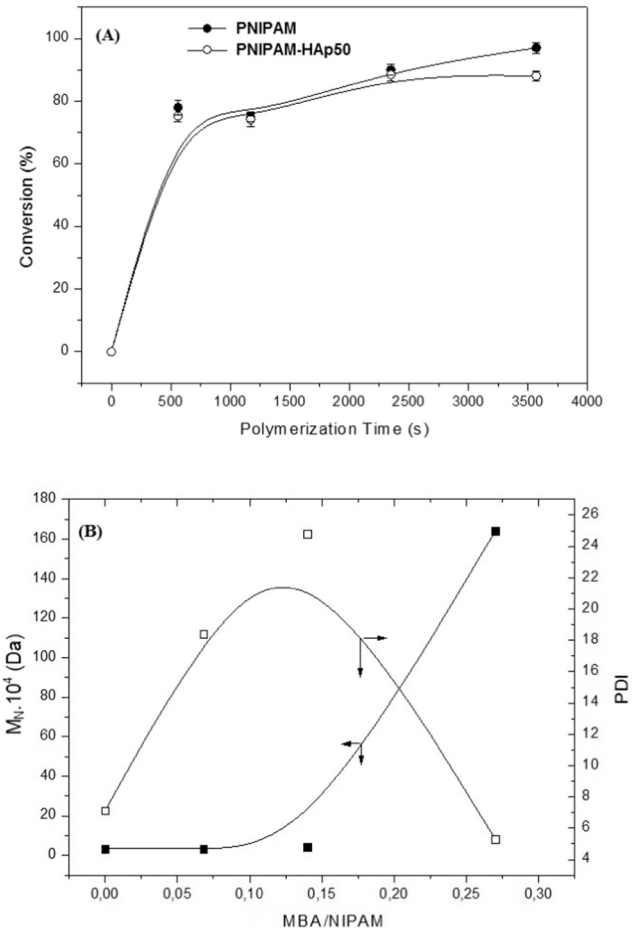

Fig. 2. The NIPAM conversion (%) as function of polymerization time at 100 mA and 25 °C (A) and the dependence of PDI and M_N of the MBA/NIPAM ratio of PNIPAM chains (B). The MBA/NIPAM solution was purged with nitrogen for 5 min before ECP. The ECP reaction was conducted at 25 °C at normal pressure and 100 mA.

thereby reducing the scaffold porosity [52].

It was found that the increase of HAp content in PNIPAM matrix results in the lowering of W_S(%) (Fig. 4(II)). This result are quite expected and may be explained by the fact that due to relatively lower hydrophilicity of the HAp relatively to PNIPAM matrix, the increasing fraction of the bioceramic in the thermoresponsive polymer results in a lower water sorption by the PNIPAM-HAp scaffold.

In order to observe the temperature dependence of the water diffusion coefficients in PNIPAM and PNIPAM-HAp scaffolds synthesized by ECP technique, experiments were conducted at two different temperatures, namely, at 25 °C and 40 °C. The diffusion coefficients (D) were calculated from Fig. 4(B) data in according to Eq. (7) [53]:

$$\frac{M_t}{M_\infty} = 2\left(\frac{D\cdot t}{\pi\cdot l^2}\right)^{1/2} \quad (7)$$

where M_t is the mass uptake at time t, M_∞ is the mass uptake at equilibrium, l is the thickness of the specimen, D is the diffusion coefficient, and t is the water uptake time.

The calculated diffusion coefficients are given in Fig. 5(A). It can be seen that the diffusion coefficient is significantly higher at high temperature of 40 °C than that at 25 °C. The activation energy (E_a) for the water diffusion in PNIPAM and PNIPAM-HAp scaffolds synthesized by ECP was calculated through the modified Arrhenius equation in according to Eq. (8):

$$\ln\frac{D_2}{D_1} = \frac{E_a}{R}\cdot\left[\frac{T_2 - T_1}{T_2\cdot T_1}\right] \quad (8)$$

where D is the diffusion coefficient, T is the absolute temperature (K), E_a is the activation energy for water diffusion (kcal·mol^{-1}) and R is the ideal gas constant (1.987 cal·K^{-1}·mol^{-1}).

The E_a calculated for the water diffusion in PNPAM and PNIPAM-HAp scaffolds synthesized through ECP technique are shown in Fig. 5(B). The experimental results suggested that E_a suffers a significantly increase with the HAp loading of PNIPAM, indicating that water diffusion appears to be easier in PNIPAM-HAp scaffolds with lower HAp content relatively to PNIPAM. This can be associated with the presence of amide group (-CONH-) in PNIPAM, which is more capable to interact with water molecules than HAp.

3.2.3. X-ray diffraction analysis (XRD)

Fig. 6 shows the XRD patterns of pure HAp (HAP-91®) and PNIPAM-HAp composites with different compositions. The peaks of pure HAp (Fig. 6(D)) around 2θ = 26° being 002 diffraction (d = 3.427) and around 2θ = 32° overlapping diffraction of 211 and 112 (d_{211} = 2.805, d_{112} = 2.778), which is consistent with the results of literature (JCPD, 9-0432). The PNIPAM exhibited two broad diffraction peaks at 2θ = 7.5° and 2θ = 20° that indicate the amorphous structure of PNIPAM (Fig. 6(A)). Fig. 6(B,C) shows the XRD peaks of the PNIPAM-HAp_{30} and PNIPAM-HAp_{50} confirming the co-presence of HAp and PNIPAM in the scaffolds, as expected. The XRD pattern of PNIPAM-

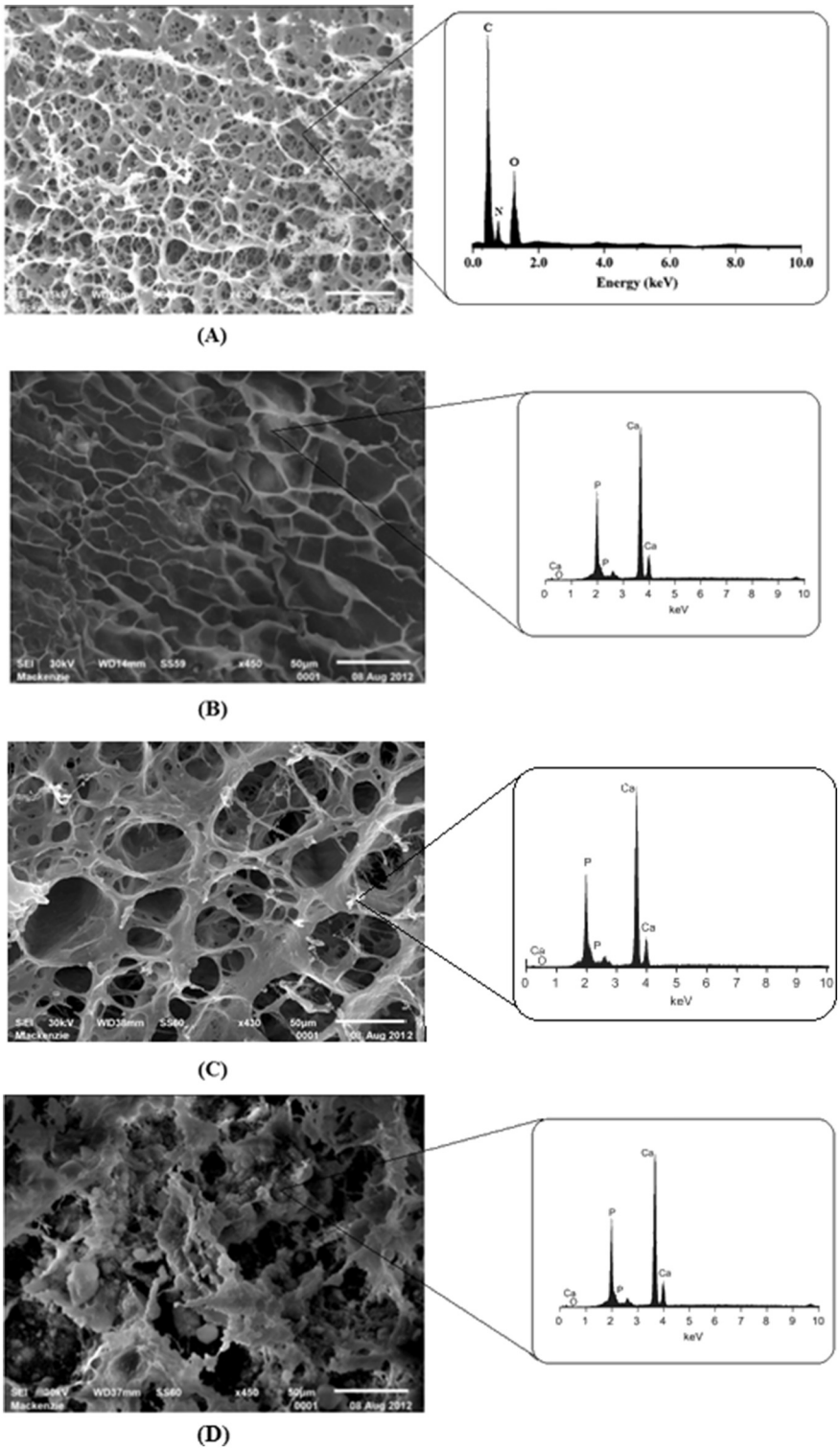

Fig. 3. SEM images of scaffolds: PNIPAM (A), PNIPAM-HAp_{30} (B), PNIPAM-HAp_{50} (C) and PNIPAM-HAp_{60} (D) with energy dispersive spectroscopy elemental composition identifying the P and Ca from the bioceramic particles.

HAp_{60} (XRD not shown) appeared similar to PNIPAM-HAp_{30} and PNIPAM-HAp_{50} scaffolds.

3.2.4. Fourier transform infrared (FTIR) spectroscopy

The FTIR spectra of PNIPAM and PNIPAM-HAp scaffolds are shown in Fig. 7. The main peak FTIR assignments are absorption bands at 3285 cm^{-1} and 3435 cm^{-1} (secondary amide N—H stretching), 2972 cm^{-1} ($-CH_3$ asymmetric stretching), 1631 cm^{-1} (secondary amide C═O stretching, amide I bond), and 1534 cm^{-1} (secondary amide C═O stretching, amide II bond). The FTIR spectrum of PNIPAM synthesized by ECP compared well with those observed in chemically synthesized thermoresponsive polymer [54].

In the spectra of PNIPAM-HAp scaffolds, the incorporation of HAp lead to the emergence of characteristic peaks assigned to HAp bands, namely the PO_4 stretching vibrations at 962 cm^{-1}, 964 cm^{-1} and 1028 cm^{-1}, respectively. The peak at 3569 cm^{-1} and 900 cm^{-1} were assigned to the presence of hydroxyl ions (^{-}OH) characteristic of HAp [55].

A comparison of FTIR/ATR spectra PNIPAM-HAp confirmed the effective existence of HAp particles surrounded by PNIPAM in the

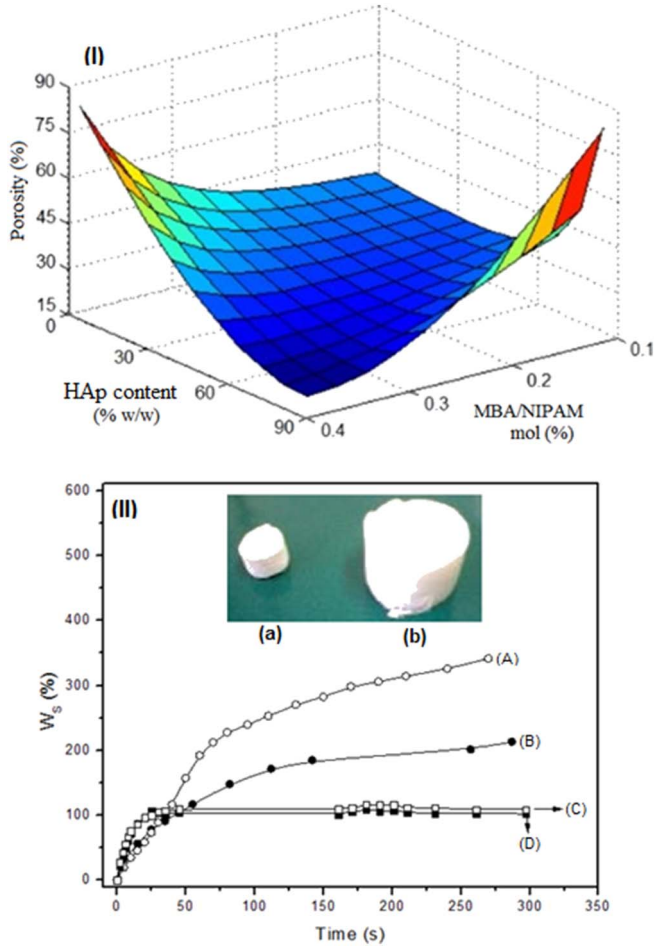

Fig. 4. Above in (I) is shown the effect of HAp content and MBA/NIPAM ratio on porosity of PNIPAM-HAp scaffolds. Below in (II) is shown the swelling isotherms (37 °C) of PNIPAM (A), PNIPAM-HAp_{30} (B), PNIPAM-HAp_{50} (C) and PNIPAM-HAp_{60} (D). Insert: photographs of the typical dry PNIPAM-HAp_{30} (a) and their respective swollen state (Q = 200% w/w) at equilibrium (t = 150 s) (b) in PBS, pH 7.4.

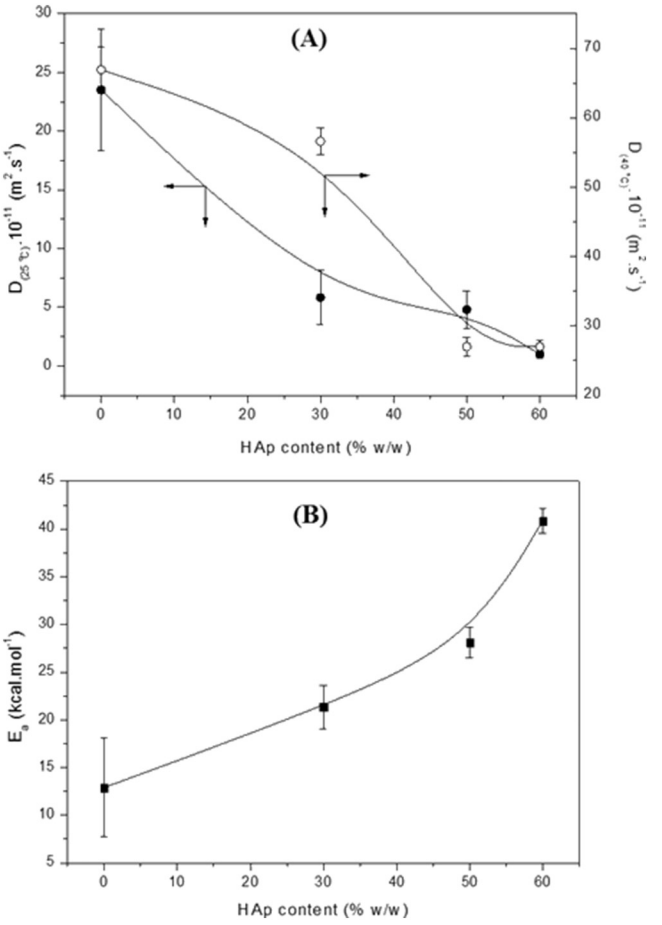

Fig. 5. Effect of hydroxyapatite content on water diffusion coefficients (D) at 25 °C (●) and 40 °C (○) (A) and the dependence of activation energy of the HAp content for water diffusion through PNIPAM-HAp scaffolds (B).

scaffolds. The feature bands for HPO_4^{2-} were assigned at 1062 cm^{-1}, 1028 cm^{-1}, 962 cm^{-1}, 964 cm^{-1} and 870 cm^{-1}. The analysis of the characteristic bands of PNIPAM in PNIPAM-HAp spectrum, showed a band shift in the wavenumber 1631 cm^{-1} (PNIPAM) to 1638 cm^{-1}. The band shifts towards higher wavenumbers suggests some interactions between PNIPAM and HAp in the PNIPAM-HAp scaffolds. Changes are observed also in a broad band in the 3000–3600 cm^{-1}. Hydrogen bonding is known to lead to shifting of the N—H deformation band to higher frequencies [56]. These changes observed in PNIPAM-HAp spectrum may be related to the establishment of weaker hydrogen bonding in the lyophilized scaffolds compared to the existent in the original PNIPAM.

3.2.5. Thermogravimetric analysis

The thermogravimetric curves (TGA) for PNIPAM and PNIPAM-HAp scaffolds with different concentrations of HAp are shown in Fig. 8. The sample of PNIPAM displays a weight loss of 16% between 25 °C and 200 °C that can be attributed to the loss of adsorbed water in polymeric matrix. The PNIPAM-HAp scaffolds show a weight loss around 4.4% for PNIPAM-HAp_{30} and 1.5% for PNIPAM-HAp_{50} and PNIPAM-HAp_{60}, respectively. The second weight loss depression for PNIPAM and PNIPAM-HAp scaffolds was appeared between about 345 °C to 450 °C due to PNIPAM backbone degradation. Using the residual weight of PNIPAM-HAp scaffolds heated to 800 °C as the reference, the amounts of HAp in PNIPAM-HAp scaffolds are 0, 28.1%, 47.5% and 58.5% for PNIPAM, PNIPAM-HAp_{30} PNIPAM-HAp_{50} and PNIPAM-HAp_{60}, respectively. The TGA results showed a good agreement with the theoretical composition of PNIPAM-HAp scaffolds, further implying that the HAp is coated with different amounts of PNIPAM via ECP polymerization.

3.3. Citotoxicity assay and oxacillin delivery

3.3.1. Cytotoxicity assay

Since PNIPAM-HAp scaffolds are materials candidates to use in bone tissue engineering, it is important to assure that no cytotoxic materials were imparted in their structure. The tetrazolium-based colorimetric assay (MTT test), a commonly used method [57], was carried out to quantitatively determine the biological response of MG63 cells to the PNIPAM-HAp composites. Fig. 9 summarizes the MTT assay results of ECP PNIPAM and PNIPAM-HAp composites. The percentages of viable cells after the exposure to various composites were above 95% in most instances throughout 24 h. The results of the cytotoxicity tests showed that there was no signification difference between PNIPAM and PNIPAM-HAp samples suggesting that the PNIPAM-HAp scaffolds synthesized through ECP process are not cytotoxic to MG63 cells reinforcing their potential use in bone tissue engineering.

3.3.2. Oxacillin release

Bone and soft tissue infections are serious problems in orthopedic and reconstructive surgery. Today it is well known that the infection in orthopedic surgeries for implant of biomaterials might be reduced through the local delivery of antibiotics at surgical sites [58]. The localized antibiotic delivery at concentrations above the minimum

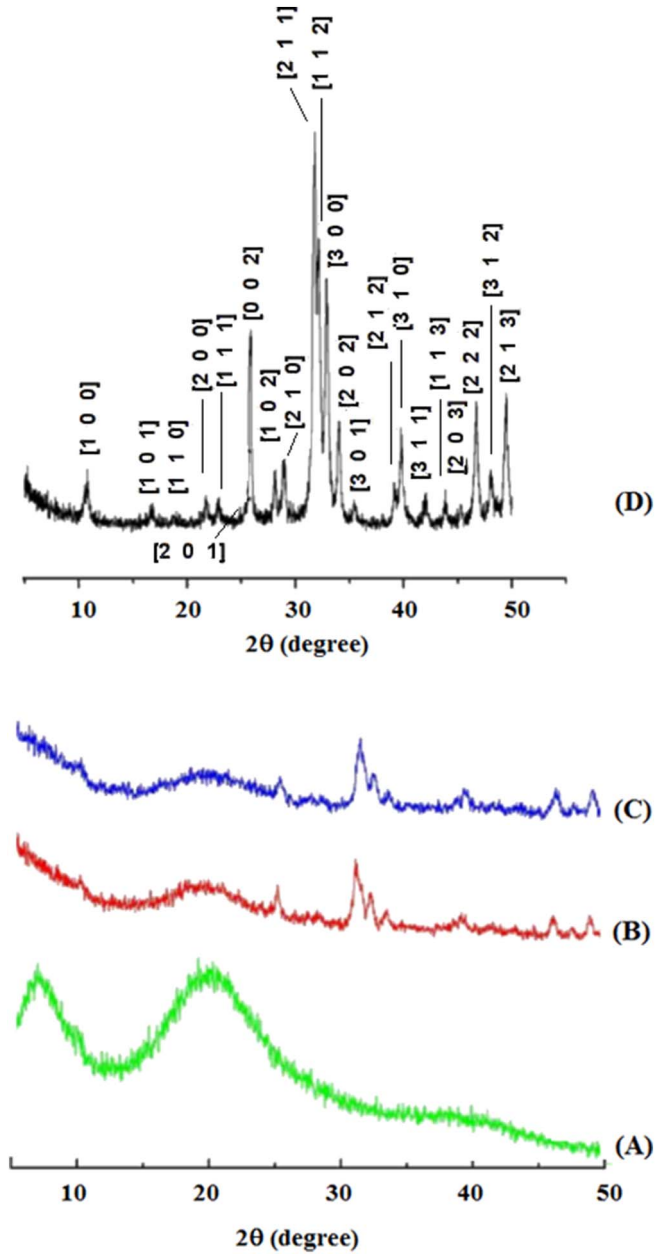

Fig. 6. XRD pattern of PNIPAM (A), PNIPAM-HAp$_{30}$ (B), PNIPAM-HAp$_{50}$ (C) and HAp (HAP-91) powder (D).

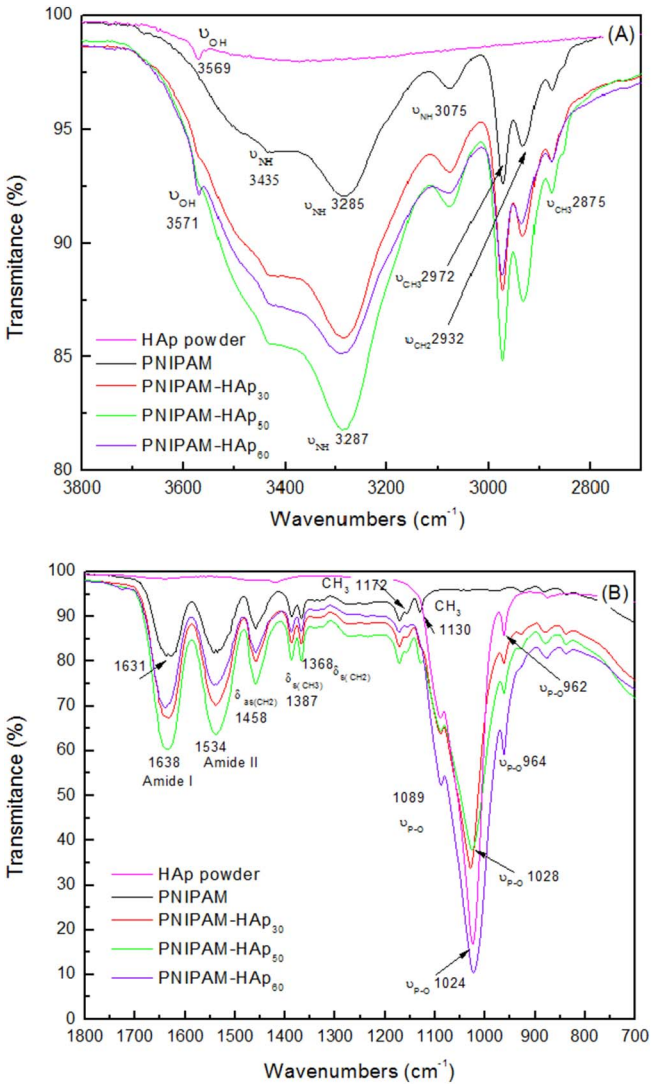

Fig. 7. FTIR/ATR spectra of PNIPAM, PNIPAM-HAp$_{30}$, PNIPAM-HAp$_{50}$ and PNIPAM-HAp$_{60}$ scaffolds synthesized by ECP technique in the range of 2800–3800 cm^{-1} (A) and in the range 700–1800 cm^{-1} (B). A standard FTIR/ATR of the HAp used in this work was used for comparison.

inhibitory concentration (MIC) at the implant site minimizes the systemic toxicity, and ensures initial drug concentrations above the MIC at the implant site.

The oxacillin loading (%w/w) and oxacillin incorporation efficiency (w/w) by PNIPAM-HAp scaffolds are represented in Fig. 10. On comparing drug loading (% w/w) and incorporation efficiency (% w/w), it was observed that significantly ($p < 0.05$) higher both drug loading (DL) (75.6 ± 0.62% w/w) and drug incorporation efficiency (IE) (86.7 ± 2.19%w/w) were observed in case of ECP PNIPAM compared to their composites PNIPAM-HAp$_{30}$ (DL = 67.3 ± 0.92% w/w, IE = 85.65 ± 1,72 w/w), PNIPAM-HAp$_{50}$ (DL = 64.2 ± 1,14% w/w, IE = 85.7% ± 2,05 w/w) and PNIPAM-HAp$_{60}$ (DL = 61.4 ± 0,78 w/w, IE = 84.7 ± 1,23 w/w). This result suggests that the increased HAp concentration leads to a decrease in the drug loading capacity of the PNIPAM scaffolds. The decrease in both, hydrophilicity and the porosity with HAp content seems to prevent the molecular movement of the oxacillin around the PNIPAM chains and entraps the antibiotic into

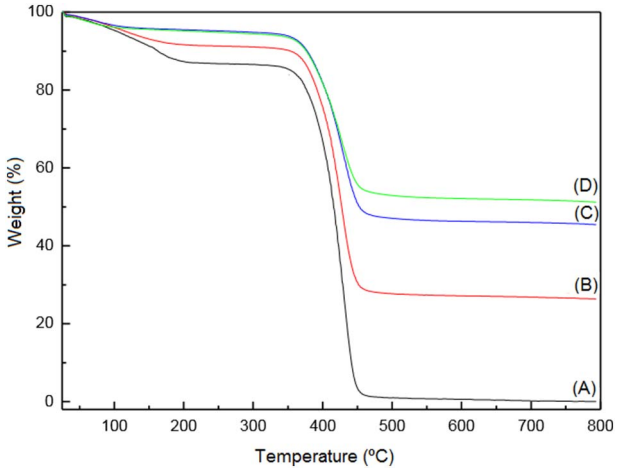

Fig. 8. Thermogravimetric analysis (TGA) of PNIPAM (A) and PNIPAM-HAp$_{30}$ (B), PNIPAM-HAp$_{50}$ (C) and PNIPAM-HAp$_{60}$ (D) scaffolds. TGA analysis was performed in air at a heating rate of 10 °C/min.

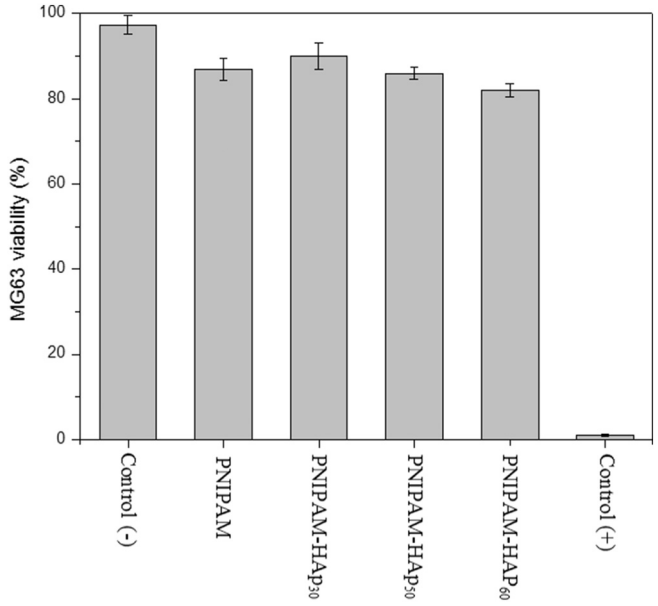

Fig. 9. Cytotoxicity assay against MG63 cells against of PNIPAM and PNIPAM-HAp scaffolds. MG63 cell populations were cultured in monolayer in DMEM (negative, non-cytotoxic control) and with extract media of PNIPAM, PNIPAM-HAp composites and phenol at 0.3% (m/v) in PBS pH 7.4 (positive, cytotoxic control).

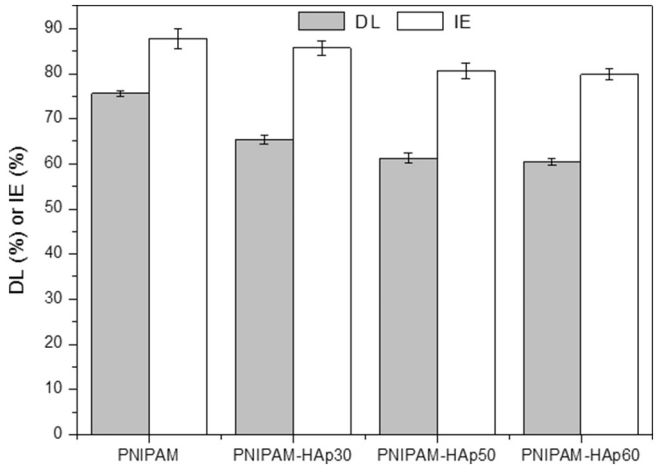

Fig. 10. Oxacillin loadings (DL, % w/w) and oxacillin incorporation efficiencies (IE, % w/w) of PNIPAM and PNIPAM-HAp scaffolds. (Mean ± SD, N = 3).

the PNIPAM-network. As a result, the drug loading capacity of the PNIPAM-HAp decreased with the increase in HAp content.

The amount of oxacillin released from PNIPAM-HAp scaffolds was measured as a function of time and the results are shown in Fig. 11. The approach applied in this study was to prepare samples with the same crosslinking density but differing in terms of the amount of hydroxyapatite in PNIPAM-HAp scaffold. The highest average concentration of oxacillin was achieved after 12 h and without the burst releasing effect for PNIPAM and PNIPAM-HAp scaffolds. The release kinetics (Fig. 11) of PNIPAM and PNIPAM-HAp scaffolds shows a rapid release of oxacillin for PNIPAM and PNIPAM-HAp_{30}. A factor that may have influenced the release of oxacillin may be the porosity of the PNIPAM-HAp scaffolds. The presence of larger pores sizes in PNIPAM and PNIPAM-HAp_{30} scaffolds results in more dissolution than diffusion hence it shows a rapid oxacillin release in the first few hours. However for PNIPAM-HAp_{50} and PNIPAM-HAp_{60} the release kinetics is found to be slightly lower for every lower concentration which may be due to the lesser pore size. This may be due to the smaller pore size presents in these scaffolds which will have lesser dissolution and more diffusion of

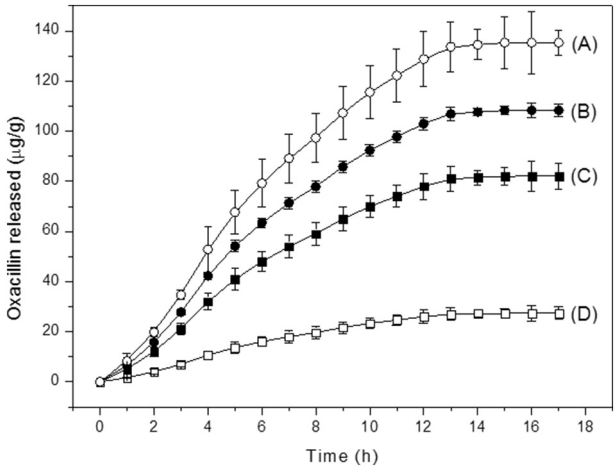

Fig. 11. Amount of the oxacillin released from PNIPAM (A), PNIPAM-HAp_{30} (B), PNIPAM-HAp_{50} (C) e PNIPAM-HAp_{60} (D) scaffolds as a function of time (n = 3).

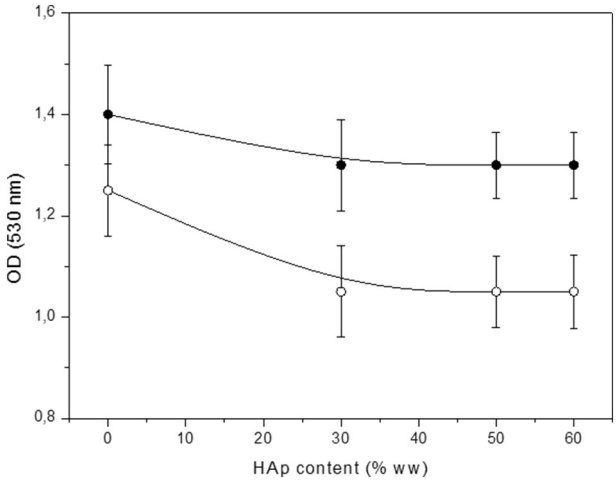

Fig. 12. Inhibitory effectiveness of the released oxacillin from PNIPAM-HAp as a function of HAp content on hydrogel measured at 530 nm against *S. aureus* (○) and *P. aeruginosa* (●) according to turbidity method after 24 h incubation.

oxacillin and hence the release is sustained.

Fig. 12 shows that the antibiotic eluted from all PNIPAM-HAp scaffolds regardless of HAp content were effective in inhibiting growth of the *S. aureus* as Gram-positive bacteria and *P. aeruginosa* as Gram-negative bacteria indicating that the oxacillin does not react or undergo inactivation by the PNIPAM-HAp scaffolds. However, the inhibition is increased with decreasing HAp content on PNIPAM-HAp composites (Fig. 12). It is possible that the oxacillin loading could explain the dependence of the bacterial inhibition zone of the PNIPAM-HAp composition. However, the interactions of oxacillin with PNIPAM-HAp scaffolds is not well known, and although in this study it was observed that the content of HAp exerts an influence on the amount of oxacillin released, the exact mechanism by which this effect occurred is not well understood nor is the purpose of this work. Future experimentation is needed to determine reasons for the dependence between the HAp content on PNIPAM-HAp scaffolds and antibiotic activity against microorganisms at inhibitory concentrations.

4. Conclusion

In this study the preparation and characterization of three-dimensional porous PNIPAM-HAp scaffolds through ECP technique for bone tissue engineering applications have been studied. SEM was used for microstructural analysis while XRD and FTIR techniques were used for

chemical analysis. By SEM it was possible to observe that the PNIPAM-HAp scaffolds are highly porous in nature and the HAp content appears to control the porosity of the composite. FTIR and XRD analysis showed that the PNIPAM-HAp scaffolds structures contained original constituents, no new chemical compounds were formed and the ECP process had not affected the crystallinity of the HAp. The TGA results are in good agreement with the theoretical composition of PNIPAM-HAp scaffolds, further implying that the HAp is coated with different amounts of PNIPAM via ECP polymerization. Biological investigations, using MTT confirmed that PNIPAM-HAp scaffolds prepared through ECP technique are not cytotoxic for MG63 cells. The PNIPAM-HAp content exerts significantly influence on oxacillin loading and in its release from PNIPAM-HAp scaffolds. The PNIPAM-HAp scaffolds with high HAp content had a lower oxacillin release rate compared to the scaffolds with low HAp content. The oxacillin released from PNIPAM-HAp scaffolds was able to sustain the bacterial activity against *S. aureus* and *P. aeruginosa*. The data obtained in this study suggests that ECP is a promising technique for the manufacture of PNIPAM-HAp scaffolds for bone tissue engineering.

Acknowledgement

The authors acknowledge the financial support from the CNPq (305894/2014-5), FAPEMIG (TEC-551/90/TEC-548/90/ PPM-00726-15), FINEP (MCT/CT-INFRA-PROINFRA-01/2004) and CAPES (REUNI/DS).

References

[1] S. Lee, T. Kwon, E.K. Chung, J.W. Lee, The market trend analysis and prospects of scaffolds for stem cells, Biomater. Res. 18 (2014) 1–10.
[2] Global Data, Bone Graft Substitutes—Global Pipeline Analysis, Competitive Landscape and Market Forecast to 2017, Global Data, London, UK, 2011.
[3] iData Research, U.S. Orthopedic Biomaterials Market, iData Research, Dallas, Tex, USA, 2013.
[4] Medtech Insight/Elsevier Business Intelligence, European markets for bone graft substitute products for spinal fusion, Tech. Rep. #A329, Life Science Intelligence, Huntington Beach, Calif, USA, 2011.
[5] J. Zhu, R.E. Marchant, Design properties of hydrogel tissue-engineering scaffolds, Expert Rev. Med. Devices 8 (2011) 607–626.
[6] K.Y. Lee, D.J. Mooney, Hydrogels for Tissue Engineering, Chem. Rev. 101 (2001) 1869–1880.
[7] J.A. Hunt, R. Chen, T. van Veen, N. Bryan, Hydrogels for tissue engineering and regenerative medicine, J. Mater. Chem. B2 (2014) 5319–5338.
[8] J.L. Drury, D.J. Mooney, Review hydrogels for tissue engineering: scaffold design variables and applications, Biomaterials 24 (2003) 4337–4351.
[9] H. Tan, K.G. Marra, Injectable, biodegradable hydrogels for tissue engineering applications, Materials 3 (2010) 1746–1767.
[10] A. Galperin, T.J. Long, B.D. Ratner, Degradable, thermo-sensitive poly(*N*-isopropyl acrylamide)-based scaffolds with controlled porosity for tissue engineering applications, Biomacromolecules 11 (2010) 2583–2592.
[11] N. Ozturk, A. Girotti, G.T. Kose, J.C. Rodríguez-Cabello, V. Hasirci, Dynamic cell culturing and its application to micropatterned elastin-like protein-modified poly (N-isopropylacrylamide) scaffolds, Biomaterials 30 (2009) 5417–5426.
[12] L. Yu, J. Ding, Injectable hydrogels as unique biomedical materials, Chem. Soc. Rev. 37 (2008) 1473–1481.
[13] A. Sivashanmugam, R.A. Kumar, M.V. Priya, S.V. Nair, R. Jayakumar, An overview of injectable polymeric hydrogels for tissue engineering, Eur. Polym. J. 72 (2015) 543–565.
[14] M.B. Dreifke, N.A. Ebraheim, A.C. Jayasuriya, Investigation of potential injectable polymeric biomaterials for bone regeneration, J. Biomed. Mater. Res. A 101 (2013) 2436–2447.
[15] G. Graziano, On the temperature-induced coil to globule transition of poly-N-isopropylacrylamide in dilute aqueous solutions, Int. J. Biol. Macromol. 27 (2000) 89–97.
[16] P. Kujawa, F. Tanaka, F.M. Winnik, Temperature-dependent properties of telechelic hydrophobically modified poly(N-isopropylacrylamides) in water: evidence from light scattering and fluorescence spectroscopy for the formation of stable mesoglobules at elevated temperatures, Macromolecules (2006) 3048–3055.
[17] K.N. Plunkett, Z. Zhu, J.S. Moore, D.E. Leckband, PNIPAM chain collapse depends on the molecular weight and grafting density, Langmuir 22 (2006) 4259–4266.
[18] H. Yamauchi, Y. Maeda, LCST and UCST behavior of poly(*N*-isopropylacrylamide) in DMSO/water mixed solvents studied by IR and micro-Raman spectroscopy, J. Phys. Chem. B 111 (2007) 12964–12968.
[19] H. Vihola, A. Laukkanen, L. Valtola, H. Tenhu, J. Hirvonen, Cytotoxicity of thermosensitive polymers poly(N-isopropylacrylamide), poly(N-vinylcaprolactam) and amphiphilically modified poly(N-vinylcaprolactam), Biomaterials 26 (2005) 3055–3064.
[20] T.T. Chastek, A. Wadajkar, K.T. Nguyen, S.D. Hudson, T.Q. Chastek, Polyglycol-templated synthesis of poly(N-isopropyl acrylamide) microgels with improved biocompatibility, Colloid Polym. Sci. 288 (2010) 105–114.
[21] N. Joseph, T. Prasad, V. Raj, P.R.A. Kumar, K. Sreenivasan, T.V. Kumary, A cytocompatible poly(N-isopropylacrylamide-co-glycidylmethacrylate) coated surface as new substrate for corneal tissue engineering, J. Bioact. Compat. Polym. 25 (2010) 58–74.
[22] S.A. Meenach, A.A. Anderson, M. Suthar, K.W. Anderson, J.Z. Hilt, Biocompatibility analysis of magnetic hydrogel nanocomposites based on poly(N-isopropylacrylamide) and iron oxide, J. Biomed. Mater. Res. 91A (2009) 59–74.
[23] M.A. Cooperstein, H.E. Canavan, Assessment of cytotoxicity of (N-isopropyl acrylamide) and poly(N-isopropyl acrylamide)-coated surfaces, Biointerphases 8 (2013) 1–12.
[24] W.H. Binder, D. Gloger, H. Weinstabl, G. Allmaier, E. Pittenauer, Telechelic poly(*N*-isopropylacrylamides) via nitroxide-mediated controlled polymerization and "click" chemistry: livingness and "grafting-from" methodology, Macromolecules 40 (2007) 3097–3107.
[25] J. Ye, R. Narain, Water-assisted atom transfer radical polymerization of *N*-isopropylacrylamide: nature of solvent and temperature, J. Phys. Chem. B 113 (2009) 676–681.
[26] A.J. Convertine, N. Ayres, C.W. Scales, A.B. Lowe, C.L. McCormick, Facile, controlled, room-temperature RAFT polymerization of *N*-Isopropylacrylamide, Biomacromolecules 5 (2004) 1177–1180.
[27] K.T. Nguyen, J.L. West, Photopolymerizable hydrogels for tissue engineering applications, Biomaterials 23 (2002) 4307–4314.
[28] Y.V. Pan, R.A. Wesley, R. Luginbuhl, D.D. Denton, B.D. Ratner, Plasma polymerized *N*-isopropylacrylamide: synthesis and characterization of a smart thermally responsive coating, Biomacromolecules 2 (2001) 32–36.
[29] T. Friedrich, B. Tieke, Intelligent hydrogels via gamma-ray induced polymerization of micellar monomer solutions and microemulsions, Macromol. Symp. 287 (2010) 16–21.
[30] K. László, K. Kosik, E. Geissler, High-sensitivity isothermal and scanning microcalorimetry in PNIPA hydrogels around the volume phase transition, Macromolecules 37 (2004) 10067–10072.
[31] X. Zhang, R. Zhuo, Y. Yang, Using mixed solvent to synthesize temperature sensitive poly(*N*-isopropylacrylamide) gel with rapid dynamics properties, Biomaterials 23 (2002) 1313–1318.
[32] I. Hamad, A.C. Hunter, J. Szebeni, S.M. Moghimi, Poly(ethylene glycol)s generate complement activation products in human serum through increased alternative pathway turnover and a MASP-2-dependent process, Mol. Immunol. 46 (2008) 225–232.
[33] D. Pissuwan, C. Boyer, K. Gunasekaran, T.P. Davis, V. Bulmus, In vitro cytotoxicity of RAFT polymers, Biomacromolecules 11 (2010) 412–420.
[34] C.-W. Chang, E. Bays, L. Tao, S.N.S. Alconcel, H.D. Maynard, Differences in cytotoxicity of poly(PEGA)s synthesized by reversible addition–fragmentation chain transfer polymerization, Chem. Commun. (2009) 3580–3582.
[35] E. De Giglio, S. Cometa, M.A. Ricci, D. Cafagna, A.M. Savino, L. Sabbatini, M. Orciani, E. Ceci, L. Novello, G.M. Tantillo, M. Mattioli-Belmonte, Ciprofloxacin-modified electrosynthesized hydrogel coatings to prevent titanium-implant-associated infections, Acta Biomater. 7 (2011) 882–891.
[36] E. De Giglio, S. Cometa, C. Satriano, L. Sabbatini, P.G. Zambonin, Electrosynthesis of hydrogel films on metal substrates for the development of coatings with tunable drug delivery performances, J. Biomed. Mater. Res. A 88A (2009) 1048–1057.
[37] S. Suzuki, Y. Ikada, Biomaterials for Surgical Operation, Springer-Verlag, New York (EUA), 2012.
[38] C.S. Hege, S.M. Schiller, Non-toxic catalysts for ring-opening polymerizations of biodegradable polymers at room temperature for biohybrid materials, Green Chem. (2014) 1410–1416.
[39] N.T. Khanarian, J. Jiang, L.Q. Wan, V.C. Mow, H.H. Lu, A hydrogel-mineral composite scaffold for osteochondral interface tissue engineering, Tissue Eng. A18 (2012) 533–545.
[40] M. D'Este, D. Eglin, Hydrogels in calcium phosphate moldable and injectable bone substitutes: sticky excipients or advanced 3-D carriers? Acta Biomater. 9 (2013) 5421–5430.
[41] N. Barbani, G.D. Guerra, C. Cristallini, P. Urciuoli, R. Avvisati, A. Sala, E. Rosellini, Hydroxyapatite/gelatin/gellan sponges as nanocomposite scaffolds for bone reconstruction, J. Mater. Sci. Mater. Med. 23 (2012) 51–61.
[42] S. Rungsiyanont, N. Dhanesuan, S. Swasdison, S. Kasugai, Evaluation of biomimetic scaffold of gelatin-hydroxyapatite crosslink as a novel scaffold for tissue engineering: biocompatibility evaluation with human PDL fibroblasts, human mesenchymal stromal cells, and primary bone cells, J. Biomater. Appl. 27 (2012) 47–54.
[43] H. Zhou, J. Lee, Nanoscale hydroxyapatite particles for bone tissue engineering, Acta Biomater. (2011) 2769–2781.
[44] E.S.R. Darley, A.P. MacGowan, Antibiotic treatment of Gram-positive bone and joint infections, J. Antimicrob. Chemother. 53 (2004) 928–935.
[45] O. Okaya, Macroporous copolymer networks, Prog. Polym. Sci. 25 (2000) 711–779.
[46] M. Kazemzadeh-Narbat, S. Noordin, B.A. Masri, D.S. Garbuz, C.O. Duncan, R.E. Hancock, R. Wang, Drug release and bone growth studies of antimicrobial peptide-loaded calcium phosphate coating on titanium, J Biomed Mater Res B Appl Biomater 100 (2012) 1344–1352.
[47] CLSI, Methods for Dilution Antimicrobial Susceptibility Tests for Bacteria That Grow Aerobically; Approved Standard-ninth Edition, CLSI Document M07-A9, Clinical and Laboratory Standards Institute, Wayne, PA, 2012.
[48] A.J. Magenau, N.C. Strandwitz, A. Gennaro, K. Matyjaszewski, Electrochemically

mediated atom transfer radical polymerization, Science 332 (2011) 81–84.
[49] J.P. Gittings, C.R. Bowen, A.C.E. Dent, I.G. Turner, F.R. Baxter, J.B. Chaudhuri, Electrical characterization of hydroxyapatite-based bioceramics, Acta Biomater. 5 (2009) 743–754.
[50] J. Sun, H. Tan, Review-alginate-based biomaterials for regenerative medicine applications, Materials 6 (2013) 1285–1309.
[51] N. Kourkoumelis, I. Balatsoukas, M. Tzaphlidou, Ca/P concentration ratio at different sites of normal and osteoporotic rabbit bones evaluated by Auger and energy dispersive X-ray spectroscopy, J. Biol. Phys. 38 (2012) 279–291.
[52] T. Douglas, E. Pamula, D. Hauk, J. Wiltfang, S. Sivananthan, E. Sherry, P.H. Warnke, Porous polymer/hydroxyapatite scaffolds: characterization and biocompatibility investigations, J. Mater. Sci. Mater. Med. 20 (2009) 1909–1915.
[53] J. Crank, G.S. Park (Eds.), Diffusion in Polymers, Academic Press, New York (EUA), 1977.
[54] B. Sun, Y. Lin, P. Wu, H.W. Siesler, A FTIR and 2D-IR spectroscopic study on the microdynamics phase separation mechanism of the poly(*N*-isopropylacrylamide) aqueous solution, Macromolecules 41 (2008) 1512–1520.
[55] S. Meejoo, W. Maneeprakorn, P. Winotai, Phase and thermal stability of nanocrystalline hydroxyapatite prepared via microwave heating, Thermochim. Acta 447 (2006) 115–120.
[56] P.M. Reddy, M. Taha, P. Venkatesu, A. Kumar, M.-J. Lee, Destruction of hydrogen bonds of poly(*N*-isopropylacrylamide) aqueous solution by trimethylamine *N*-oxide, J. Chem. Phys. 136 (2012) 234904.
[57] ISO 10993-5, Biological Evaluation of Medical Devices — Part 5: Tests for In Vitro Cytotoxicity, ANSI/AAMI, Arlington VA, 2009 (2009).
[58] B.D. Brooks, S.N. Davidoff, D.W. Grainger, A.E. Brooks, Comparisons of release of several antibiotics from antimicrobial polymer-coated allograft bone void filler, Int. J. Biomed. Mater. Res. 1 (2013) 21–25.